SCIENTIFIC REPORTS

OPEN

SUBJECT AREAS:
MECHANICAL ENGINEERING
MICROFLUIDICS

Received
12 December 2013

Accepted
11 March 2014

Published
31 March 2014

Correspondence and requests for materials should be addressed to W.H.L. (weihuali@uow.edu.au) or N.-T.N. (nam-trung.nguyen@griffith.edu.au)

Inertial particle separation by differential equilibrium positions in a symmetrical serpentine micro-channel

Jun Zhang[1], Sheng Yan[1], Ronald Sluyter[2,3], Weihua Li[1], Gursel Alici[1] & Nam-Trung Nguyen[4]

[1]School of Mechanical, Materials and Mechatronic Engineering, University of Wollongong, Wollongong, NSW 2522, Australia, [2]School of Biological Sciences, University of Wollongong, Wollongong, NSW 2522, Australia, [3]Illawarra Health and Medical Research Institute, Wollongong, NSW 2522, Australia, [4]Queensland Micro and Nanotechnology Centre, Griffith University, Brisbane QLD 4111, Australia.

This paper presents an inertial microfluidic device with a simple serpentine micro-channel to continuously separate particles with high performance. Separation of micro/nano-particles has a variety of potential applications in biomedicine and industry. Among the existing separation technologies, a label-free technique without the use of antibody affinity, filter or centrifugation is highly desired to ensure minimal damage and alteration to the cells. Inertial microfluidics utilising hydrodynamic forces to separate particles is one of the most suitable label-free technologies with a high throughput. Our separation concept relies on size-based differential equilibrium positions of the particles perpendicular to the flow. Highly efficient separation is demonstrated with particles of different sizes. The results indicate that the proposed device has an integrative advantage to the existing microfluidic separation techniques, taking accounts of purity, efficiency, parallelizability, footprint, throughput and resolution. Our device is expected to be a good alternative to conventional separation methods for sample preparation and clinical diagnosis.

Particle separation has a wide range of industrial, biomedical and clinical applications such as wastewater purification, blood sample preparation and disease diagnosis[1]. Conventional macro-scale techniques such as physical filter and differential centrifugation have been used for this purpose. However, centrifugation is bulky, expensive, labour intensive and even dangerous because it contains components moving at high speed[2–3]. Centrifugation is also limited by the heterogeneity of sample source. Furthermore, exposure to a high acceleration will likely alter the immunophenotype[4] and viability[5] of cells. Physical filters are prone to clogging, and frequent cleaning is labour intensive. Thus, a simple, low cost, more efficient and less offensive technique is desired. The recently emerged microfluidic technology is endeavoured to satisfy these demands.

In microfluidics, continuous flow separation and sorting of particles are generally based on two basic concepts: the equilibrium separation and the kinetic separation[6–7]. In the first concept, particles occupy different property-dependent equilibrium positions; whereas the second concept employs different transport speeds perpendicular to primary flow direction under an applied force field[3]. According to the manipulation force, particle separation can be categorized as active and passive techniques. Active techniques depend on external force fields[8–15]. The input flow rate and throughput are rather low because target particles need a long residence time to be exposed to the force field. The auxiliary system supplying the force field further complicates the design, although it may bring flexibility and controllability to the device. In contrast, passive techniques only rely on intrinsic hydrodynamic forces or channel geometry[16–20]. Passive devices are simple and could provide a much higher throughput. As a passive technique, inertial microfluidics employing inertial migration[21] and inertial effects of fluid (secondary flow)[20] and particles (centrifugal force)[22] under a high flow speed can provide excellent separation efficiency and purity with a massive throughput. Inertial microfluidics is also label-free, which eliminates the need for potentially cell-damaging immunolabelling procedures, and promises a cost-effective cell separation method for downstream biological assays[23]. Generally, there are 6 criteria to evaluate inertial microfluidic separation/sorting device. (i) Footprint. A small device footprint not only reduces the fabrication cost, but also improves the portability. (ii) Throughput. High throughput is essential in processing a large volume of sample, and it is actually the main advantage of inertial microfluidics. (iii) Parallelizability. An effective method to amplify the throughput is to pattern parallel channels in the same device. Basically, a microchannel with linear structure (e.g. straight or serpentine) is prone to be parallelised. (iv) Performance. High separation purity and efficiency (or recovery ratio)

are important for the downstream application, including enumeration, molecular assay and drug screening, etc. (v) Resolution. The minimum particle property (size, deformability and shape) difference required to achieve effective particle separation. (vi) Complexity. Sheath flow and complicated microchannel structure (e.g. double layer microchannel) are not in favour of fabrication costs and portability. Although great progress in the inertial microfludics has been achieved recently[24–27], so far there is still lack of techniques with an integrative ability to satisfy all the required criteria simultaneously.

There are four basic types of microchannel structures used in inertial microfluidics: straight channel[24,28], expansion-contraction array channel[29–30], spiral channel[26,31] and serpentine channel[3]. Lee et al. reported a series of particle separation in an expansion-contraction array (CEA) channel, including polystyrene beads of 4 μm and 10 μm in diameter[32], blood plasma from red blood cells[33] and cancer cells from whole blood[29]. These devices can handle highly concentrated bio-particle samples such as undiluted whole blood (1×10^9 counts/ml) using a sheath flow. However, the inclusion of a sheath flow will certainly complicate the whole system, diluting the sample and potentially causing contamination. In addition, microvortex-aided trapping and separation in the similar microchannels was also developed[27,34–37]. It is believed as one of most size-sensitive separation methods which employs size-selective trapping of microvortex within expansion-contraction chambers[24]. The group of Di Carlo has conducted a series of investigation on its trapping sensitivity and efficiency by a variety of bio-samples, including cancer cells spiked in blood[34], pleural fluids[37] and blood sample[27] from cancer patients. This device basically works in batch procedures, and specifically effective in trapping of rare cells (e.g. CTCs), due to limited capacity in expansion-contraction chambers. Later, Wang et al.[36] proposed a modified microvortex-aided device by adding a side outlet in each chamber to continuously siphon larger particles from chambers, facilitating high efficiency and high purity size-based particle separation in a continuous manner. Although with great separation performance achieved, this kind of devices is still facing challenges about separation of smaller particles, as their functional cut-off size is relatively large (15 μm in diameter[34,37] and 20 μm in diameter[36]).

Spiral channels were investigated extensively for particle separation by Papautsky's group[31,38], Go's group[39], Jiang's group[40–41] and Han's group[26,42–44], etc. Kuntaegowdanahalli et al.[38] demonstrated continuous separation of three different-sized polystyrene beads (10, 15 and 20 μm in diameter) with an efficiency of 90% and a throughput of 1×10^6 cells/min. Later, Hou et al.[42] employed a similar spiral channel to isolate CTCs from blood, and achieved a recovery rate of more than 85%. Apart from that, a clinical validation with positive detection of CTCs from all the blood samples of cancer patients was reported[42]. At the same time, Guan et al.[43] introduced a novel spiral micro-channel with a trapezoidal cross-section and showed a higher separation resolution than those with rectangular cross-section. Later, isolation CTCs from cancer patient blood samples was demonstrated by this slanted spiral micro-channel[26] from the same group. A high throughput of 1.7 ml/min and increased CTC capture efficiency were achieved. Although the spiral micro-channel has a great potential for real clinical application, its throughput is still limited due to difficulties in parallelisation. A linear channel structure is more preferred for parallelization design.

Mach and Di Carlo[28] reported a massively parallelized microfluidic device that passively separates pathogenic bacteria from diluted blood. The device consists of 40 single straight micro-channels placed as a radial array. Each single channel consists of three different cross-sections, and uses a unique differential transit time by size-dependent inertial lift forces to obtain cell separation. Zhou et al.[24] utilized a more polished design of size and length for their cascaded straight channels. The separation concept is based on their theory of two-stage inertial migration which permits precise prediction of particle or cell position within the micro-channel. A much higher separation efficiency (~ 99%) and purity (~ 90%) were achieved. However, the sizes (width × height) of channel cross-section (27 μm × 50 μm upstream segment, 100 μm × 50 μm downstream segment for separation of 9.94 μm and 20 μm particles) were restrained to provide enough lateral inertial lift force. The small cross section leads to a high fluidic resistance, which needs more power to pump the sample into the microfluidic device. In addition, the channel is relatively long (>36 mm) leading to a large device footprint.

In terms of small footprint and easy parallelization, a serpentine channel with linear structure is an optimal choice. A serpentine channel not only is easy to parallelise, but also can achieve focusing and separation within a much shorter length due to the assistance of secondary flow[22,45]. Unfortunately, little effort has been paid to separate particles by a serpentine channel in inertial microfluidics. Besides a complicated hybrid microfluidic device which combines hydrodynamic size-based deterministic lateral displacement, inertial focusing in an asymmetric serpentine channel and magnetophoresis to separate cancer cells from leukocytes[46], only one attempt to develop an inertial filtration device using an asymmetrical serpentine channel was reported[3]. In this filtration system, large particles were well focused and small particles below a threshold remained unfocused and randomly distributed. Therefore, large particles were completely removed from the mixture, leaving behind small particles with a high purity (90%–100%). However, because small particles are still unfocused, plenty of them will enter the reservoirs meant for large particles, leading to undesirable purity (~20%) of large particles collection. Also the recovery efficiency of small particles was low (~56%). Ambitious work is still needed to separate binary particles mixture with high purity and high efficiency.

In order to provide a continuous separation technique with high-throughput, good parallelizability, small footprint and high separation performance, we proposed an innovative inertial microfluidic device which can continuously separate particles based on the size-dependent differential equilibrium positions. The differential focusing phenomenon is partially based on the concept of our previous study[47], where both Dean drag force and particle centrifugal force (DC force) dominate particles migration in a serpentine channel. A single focusing streak can be achieved at the centre of the channel. As inertial lift force, Dean drag force and particle centrifugal force scale differently with the particle size. Particles below a certain threshold could be dominated by the inertial lift force, and are focused along two sides of the channel. Therefore, a complete separation can be achieved with a proper outlet system. First, we examined the focusing pattern of different-sized particles under varying conditions. The results were placed into the Reynolds number - particle size operation space. After that, the available working area for particle separation can be easily determined. Then, we tested the separation of two pairs of polystyrene particle mixtures (3-μm/10-μm, and 5-μm/13-μm particles). We achieved a very high purity of both small particles (>99%) and large particles (>90%) after a single separation process at a flow rate of 600 μl/min. Finally, we successfully demonstrated the separation of biological particles (erythroleukemia cells and 5-μm polystyrene particles, and human blood cells and erythroleukemia cells) with outstanding performance.

Results

Three different focusing patterns in a serpentine channel. When the flow rate was increased from 100 μl/min to 1000 μl/min, three different particle focusing patterns were observed in a serpentine channel. If the flow condition was below a threshold A, particles were focused along the two sides of the channel. The distances between the focused streaks and the side walls were both around 38 μm (19% channel width), which was close to the reported inertial equilibrium positions in a straight channel[25,32,48], so we

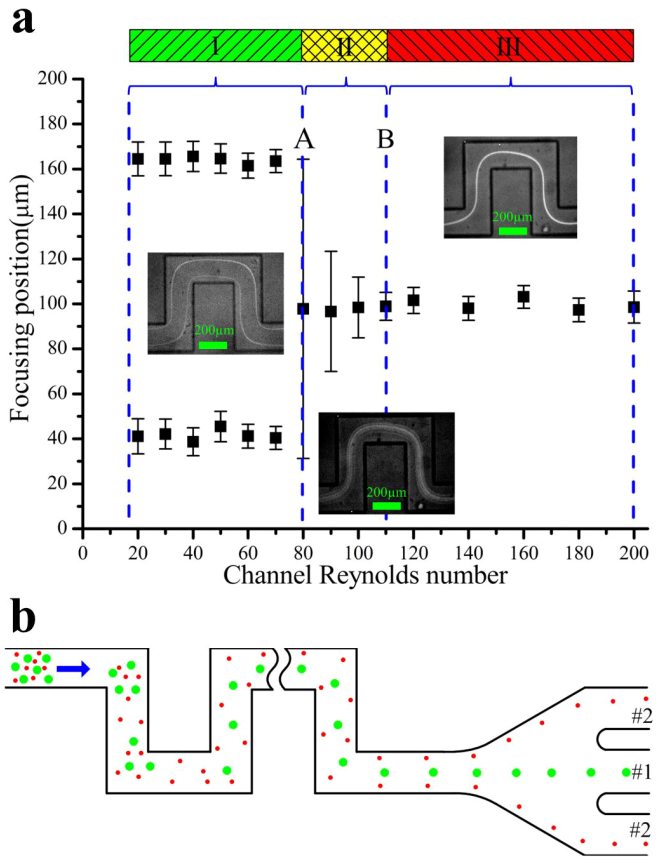

Figure 1 | (a) Three different particle focusing patterns in a serpentine channel with varying flow conditions, (I) Inertial lift force dominated region with two-sided focusing streaks, (II) transition region with a wide single central focusing band, and (III) DC dominated region with a single focusing streak at the channel centre. The error bars indicate the width of the focusing streak. Particle diameter is 10 μm. (b) Schematic illustration of particle size-based separation concept in a serpentine channel.

expected that the observed two-sided focusing is an inertial lift force dominated phenomenon. Under this flow condition (region I in Fig. 1a), inertial lift force was stronger than the DC force, and dominated the final equilibrium positions of particles. In our previous test with a straight channel of the same cross section, distinct focusing positions were not apparent even after a channel length of 40 mm. This is due to the insufficient inertial lift force to push particles to their inertial equilibrium positions within 40 mm length (supplementary Fig. S1a), and maybe a longer channel is needed. While, in a serpentine channel, these focusing positions were obvious within a much shorter channel length of 10 mm as shown in supplementary Fig. S1(b). Probably due to the combined effect of Dean flow and centrifuge force, particles can reach stable inertial equilibrium positions more quickly[22]. When flow condition exceeded a level B (region III in Fig. 1a), we proved in our previous study that the resultant effect of DC force was much greater than the inertial lift force in the serpentine channel, and a single focusing position along the channel centre can be achieved[47]. When the flow was in the region between A and B (region II in Fig. 1a), a transition phenomenon occurred. The inertial lift force and the DC force were of the same order of magnitude, and competed against each other. Particles occupied the space between the two streaks and formed a single but wide streak band. The focused streaks approached the channel centre symmetrically as the flow rate increased, and finally formed a stable single streak, where DC force began to dominate the movement of particles. The areas of regions I and III depend on the particle size. Generally, large particles have a wider region III, and a lower threshold B. Small particles have a wider region I, and a higher threshold A. If there is any overlap between these two regions ($A_{p1} \geq B_{p2}$) for two different particle sizes, the complete separation of particles is possible, according to their differential equilibrium positions along the channel width (Fig. 1b). The size-based separation mechanism proposed in the present paper is built upon the above phenomenon.

Differential equilibrium positions of different-sized particles. In order to determine the working conditions for complete particle separation, particles with a series of sizes were tested in the serpentine channel. Fluorescent streak images of different-sized particles at the outlet are plotted in Figure 2a, which shows that smaller particles had a wider region I, and particles were occupying two sides of the

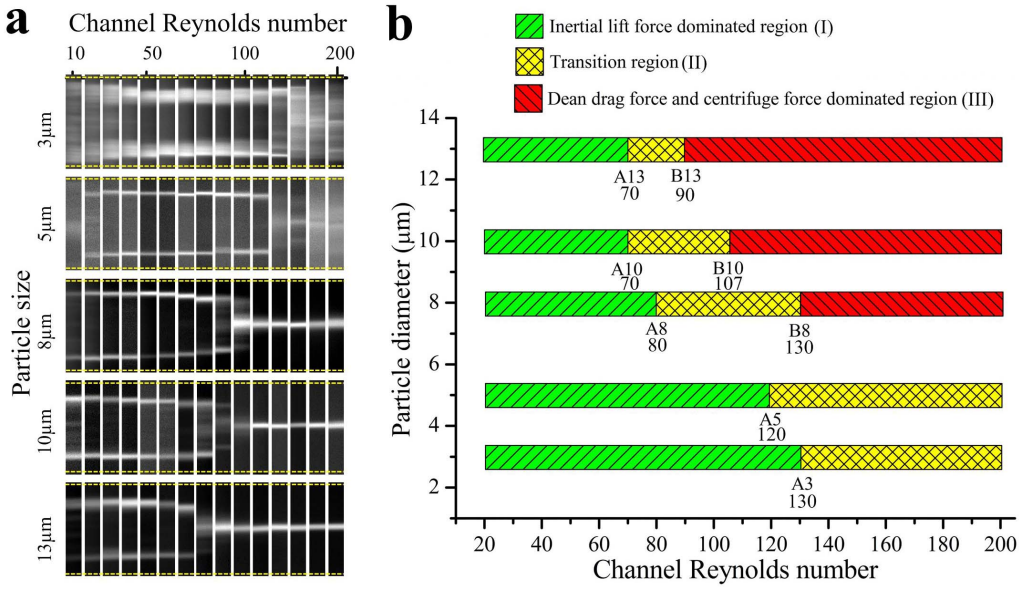

Figure 2 | **(a) Experimental observation of outlet fluorescent streak images for different-sized particles under various flow conditions; (b) Translation of particle focusing pattern into three standard regions in the channel Reynolds number – particles diameter space.**

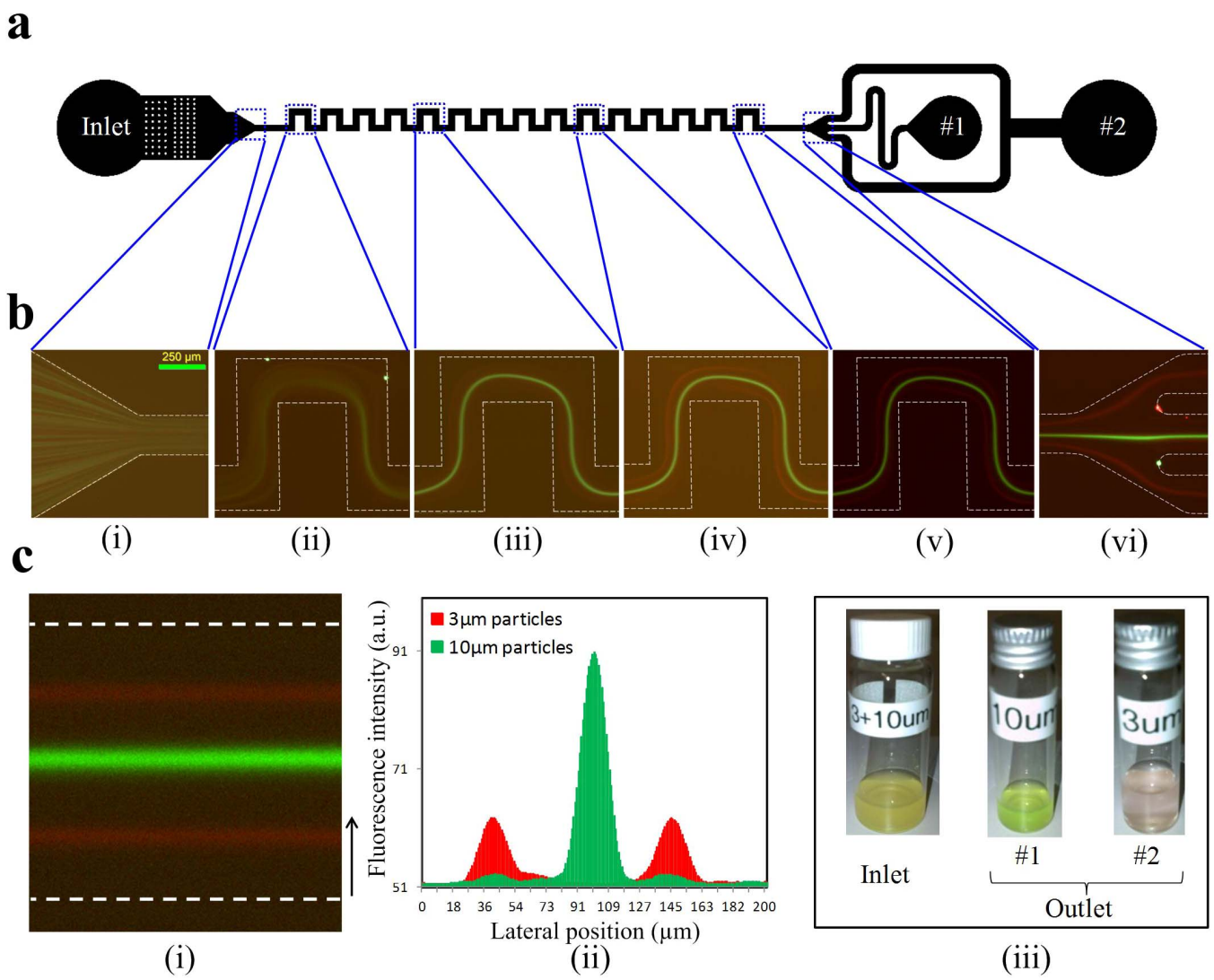

Figure 3 | (a) Schematic illustration of the micro-channel structure used for particle separation in this work. A filter upstream of the serpentine channel prevents the channel from being blocked by large debris. A trifurcation outlet system with two symmetrical side branches merged together as a single outlet #2 was used. (b) Superimposed fluorescent images illustrating the distribution and position of the 10-μm (pseudo-colored green) and 3-μm (pseudo-colored red) particles in different periods of serpentine channel. (c) (i) Fluorescent images of the particle mixture at the outlet of the serpentine channel, and (ii) its cross sectional fluorescence intensity profile presents differential equilibrium positions for binary particles. (iii) Pictures of particles suspension before and after processing indicate an effective particle separation in the serpentine channel.

channel. A more intriguing phenomenon was that small particles (≤5 μm) become unfocused rather than focused into the centre of the channel even at a large Reynolds number (Re_C = 160~200), which was different from their large counterparts (≥8 μm). Two effects are responsible for this phenomenon. First, mixing effects of Dean vortex were more effective on small particles. Small particles were prone to being retained by the counter-rotating streamlines of a Dean vortex, so that focusing at the centre of the channel is hard to be obtained. Yoon et al.[39] demonstrated that particles smaller than 27% of the channel height posed an inward velocity due to the mixing effects in a curved channel. We recently found that this ratio could be as small as 20% in a low-aspect-ratio serpentine channel, due to the suppression on mixing streamlines[47]. In this work, the channel height was 42 μm, so particles smaller than 8 μm were prone to being affected by the mixing effects of Dean flow. Therefore, the theory of Dean drag force and particle centrifugal force (DC force) induced central focusing may be not suitable for these small particles. Second, even at our high testing flow condition, DC force maybe still cannot overcome inertial lift force, so that this defocusing status could remain longer downstream. Unfortunately, it is impossible to scale these forces quantitatively to determine the particle size threshold. Particles are unstable within channel cross-section, and their movement speed and direction along channel cross-section is uncertain, causing varying Dean drag force. Moreover, the exact mechanism how Dean drag force and particle centrifuge force collaborate together to fight against inertial lift force is still unclear.

The focusing pattern of different-sized particles was placed into three standard regions, and plotted in the channel Reynolds number versus particles size operation map (Fig. 2b), which indicates the available working area for the separation of particles with specific sizes. The operation map shows a distinct overlap between region I of 3 μm and 5 μm particles and region III of 10 μm and 13 μm particles. The transition threshold A for 3 μm (A3 = 130) and 5 μm (A5 = 120) particles was obviously higher than the transition threshold B for 10 μm (B10 = 107) and 13 μm (B13 = 90) particles. So it is possible to completely separate particles based on their size-dependent differential equilibrium positions in the serpentine channel, a fact that will be demonstrated in the following sections. The quantitative particle

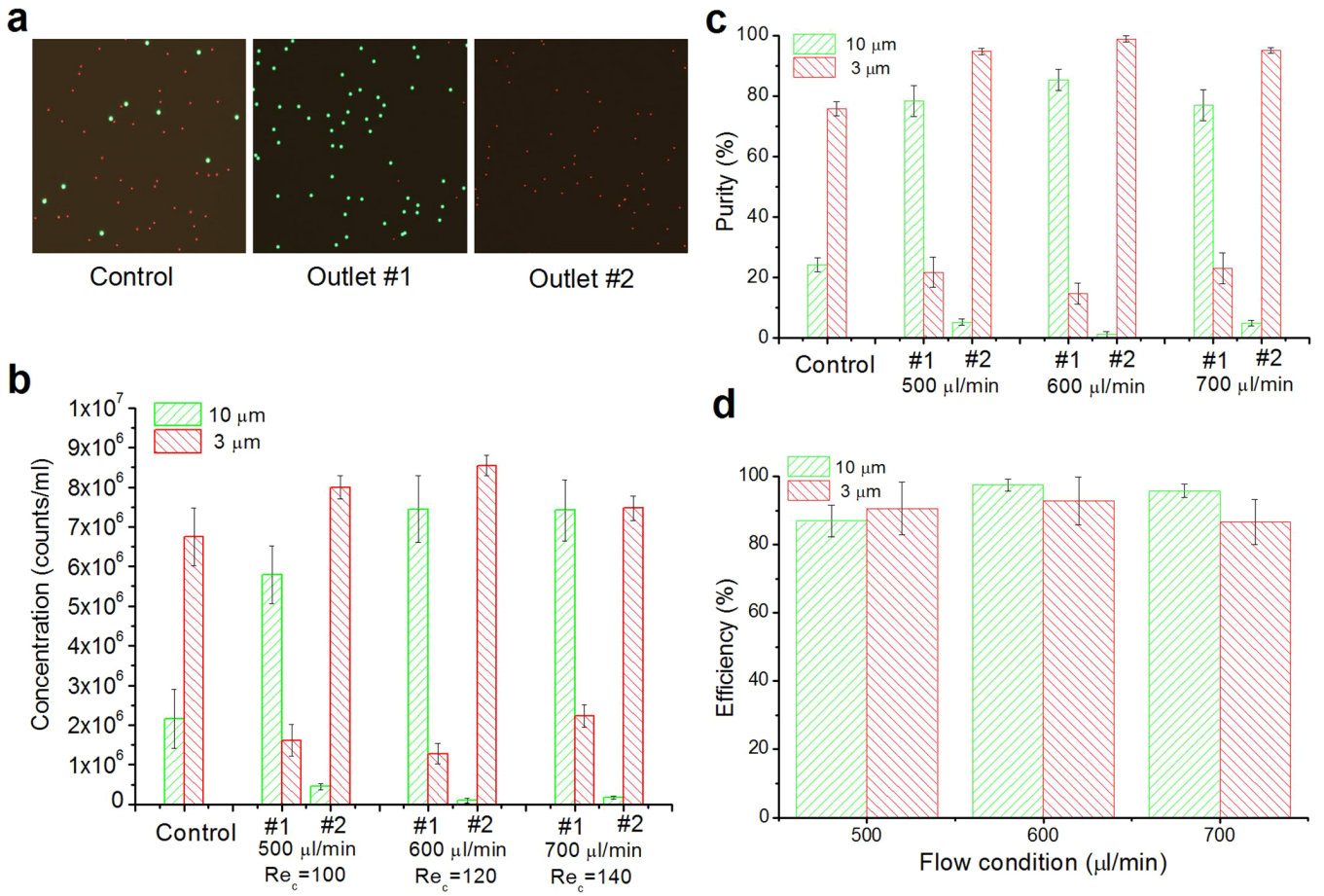

Figure 4 | Separation of 3 μm and 10 μm particles in the serpentine channel. (a) Fluorescent images of collections from control and two outlets. The control is particle mixture collected before passing through the serpentine channel. Pseudo-colored green and red dots represent 10 μm and 3 μm particles respectively. (b) Particle concentrations from control and two outlets under different processing flow conditions (flow rate or Reynolds number). (c) The purity of particles from two collectors at various flow conditions. (d) The separation efficiency for 3-μm and 10-μm particles under different flow conditions. Error bars represent the standard deviation of three measurements by hemocytometry.

streak position and width under various flow conditions were shown in supplementary Fig. S2. The streak position is not only useful for the determination of the available flow condition, but also important for designing a proper outlet system for particle separation.

Separation of polystyrene particles. A mixture of fluorescent particles with diameters of 3 μm and 10 μm were tested in the designed device to demonstrate the concept of complete separation. Figure 3a is a schematic illustration of microchannel structure used for particle separation in the present work. Pillar arrays acting as a filter upstream of the serpentine channel was used to prevent clogging by large debris. A trifurcating outlet system was placed at the end of serpentine channel. For simple handling, the two symmetrical side branches were merged together into a single outlet.

The fluorescent images of particles at different periods in the serpentine channel are shown in Figure 3b. Particles were randomly distributed at the channel inlet [Fig. 3b(i)]. After passing through several serpentine periods, large particles migrated into the channel centre dominated by the DC force, while small particles occupied two sides of the channel due to the dominant inertial lift force [Fig. 3b(ii~v)]. At the end, a three-branch outlet system was used to collect particles from different lateral positions [Fig. 3b(vi)]. Figure 3c(i) shows the distribution and position of 10-μm and 3-μm particles before the trifurcation. The fluorescence intensity profile clearly demonstrates distinct lateral positions of 10-μm and 3-μm particles [Fig. 3c(ii)], facilitating particle separation by size. Figure 3c(iii) shows particle suspensions before and after the treatment by the microfluidic device, clearly indicates an effective separation for the particles mixture.

The particles mixture was tested in the microfluidic device with different throughputs to quantitatively evaluate the separation performance. Particle concentration, particle purity (collected target particle number/collected total number[24]) and separation efficiency (collected target particle number/input target particle number[1,49]) were measured and shown in Figures 4b~d, respectively. The sample collected from outlet #2 had a very high purity (~99%) of small 3-μm particles, due to excellent focusing of larger 10-μm particles at the channel centre. However, for collection from outlet #1, purity of large 10-μm particles was not as high as expected. The maximum purity was around 88.7%, although this value was much greater than the input purity of 24.2%. The main reason is that small 3-μm particles still could not experience enough inertial lift force in the migration process even with the assistance of DC force. There was no distinct single lateral equilibrium position for them, but a wide band area (Fig. 2a). The wide band reduced the separation distance between large and small particles along the lateral direction, and increased the possibility of small particles entering outlet #1, finally deteriorated the purity of the collected large 10-μm particles. In addition, the separation efficiencies for both large particles and small particles are more than 90% (97.5% for 10-μm particles and 92.8% for 3-μm particles), which implies that most input particles can be effectively separated and recovered at their corresponding collectors.

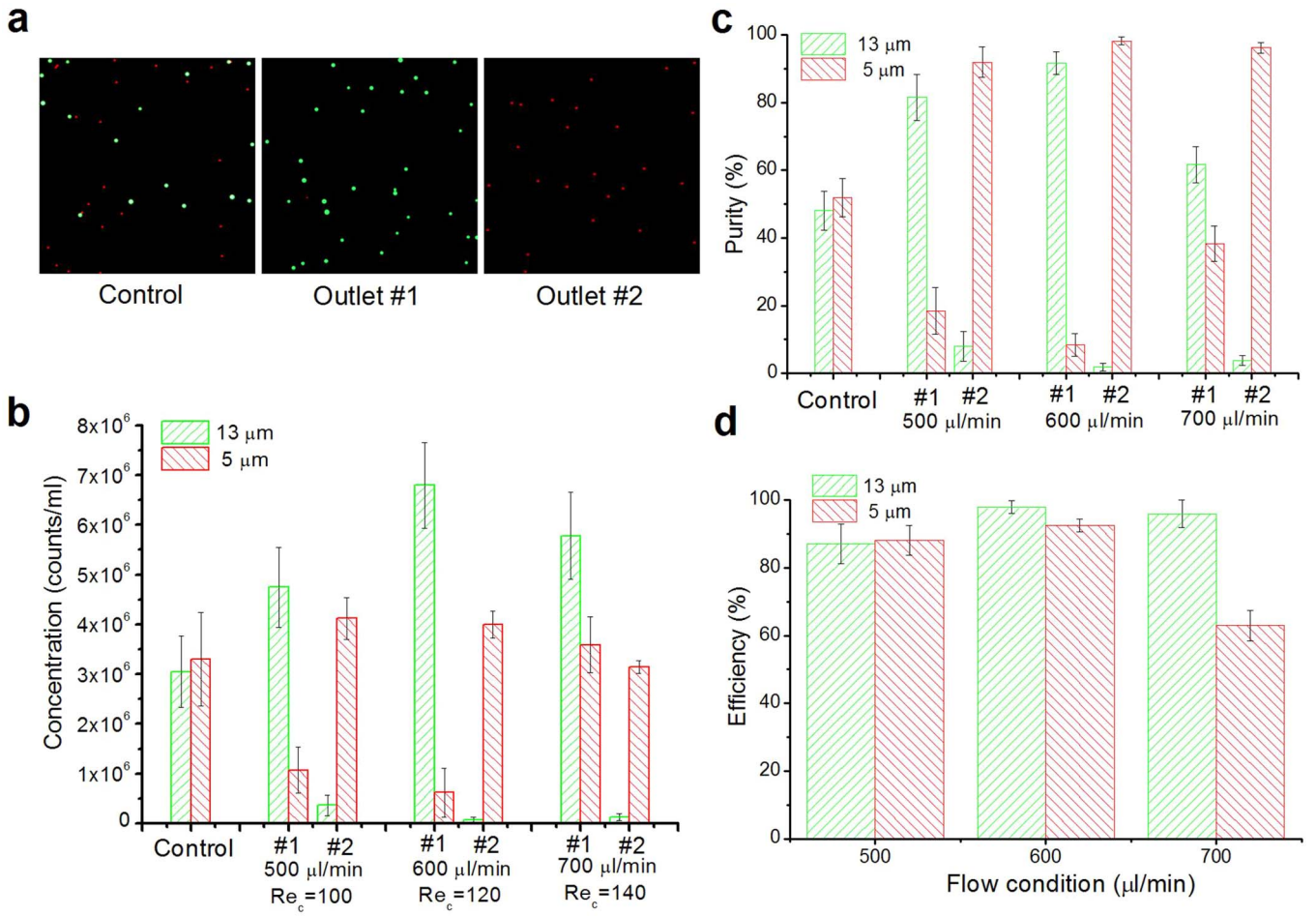

Figure 5 | Separation of 5-μm and 13-μm particles in the serpentine channel. (a) Fluorescent images of collections from control and two outlets. Pseudo-colored green and red dots represent 13-μm and 5-μm particles respectively. (b) Particle concentrations from control and two outlets under three different processing flow conditions. (c) The purity of particles from two collectors at various flow conditions. (d) The separation efficiency for 5-μm and 13-μm particles under different flow conditions. Error bars represent the standard deviation of three measurements by hemocytometry.

We also tested the separation of a mixture of 5-μm and 13-μm particles. Since 5-μm particles had a larger size and experienced a much larger inertial lift force (F_L) and DC force (F_D & F_{cent}) as well as a faster lateral migration speed than 3-μm particles, two narrow focusing streaks along the channel could be observed in Figure 2a. As expected, at the optimal flow rate (600 μl/min), the purity of large 13-μm particles collected at outlet #1 could be as high as 91.6%. Small 5-μm particles collected at outlet #2 (Fig. 5c) also achieved a high separation purity of more than 99.2%. The fluorescent images of particles from the control and outlets in the hemocytometer showed the excellent separation performance of our device (Fig. 5a). It should be noted that the purity of collected particles sample is taken from a single process, so it is expected that complete separation with purity of more than 99% could be obtained with a cascading process.

Separation of biological particles. *Murine erythroleukemia (MEL) cells and 5-μm polystyrene beads*. MEL cells, as a commonly used model of red blood cell biology[50–51], are used to investigate molecular events involved in the oncogenesis of erythroleukemias[52]. Microscopic measurements of 70 randomly selected MEL cells revealed that live MEL cells have a mean diameter ~12.6 μm with a standard deviation of ~2 μm. In order to test the separation capacity of our device on biological cells, MEL cells were mixed with 5 μm polystyrene particles at a ratio of ~1 : 1 in PBS solution. The mixture was then pumped into the microfluidic device under the optimal flow rate of 600 μl/min. Beads and MEL cells concentration and purity from input mixture and two collections from outlets were plotted in Figures 6a and 6b. Their bright field and fluorescent images were shown in supplementary Fig. S3. Within our expectations, sample collected from outlet #2 resulted in a very high purity (~98%) of 5-μm particles. Also, a high purity of ~94.9% was also achieved for MEL cells obtained from outlet #1. The flow cytometric data (plotted as forward scatter FSC and side scatter SSC) were shown in Figure 6c, which further supports the high separation performance of our device. Additionally, MEL cells were spiked into the human blood sample as a model of circulating tumours cells. The ratio of MEL cells to human blood cells was set as 1 : 100, and the concentration of the whole cells was around 5×10^7/ml. The results of separation of MEL cells from human blood cells in a single process were plotted in supplementary Fig. S4. The purity of MEL cells can be improved from 1.25% to 45.4%, indicating an effective isolation and enrichment of MEL cells. And it demonstrated the ability of our device on the separation and isolation of CTCs from cancer patients' blood sample for the diagnosis and prognosis.

Discussion

Particle separation in the device reported here relies on the overlap area between inertial lift force dominated region (region I) and DC dominated region (region III) for different-sized particles (Fig. 2b). Normally, small particles have a wider region I, and large particles have a wider region III. The overlap between these areas is the working space available for particle separation. It should be noted that the particle mixture is assumed to be diluted, and particle-particle

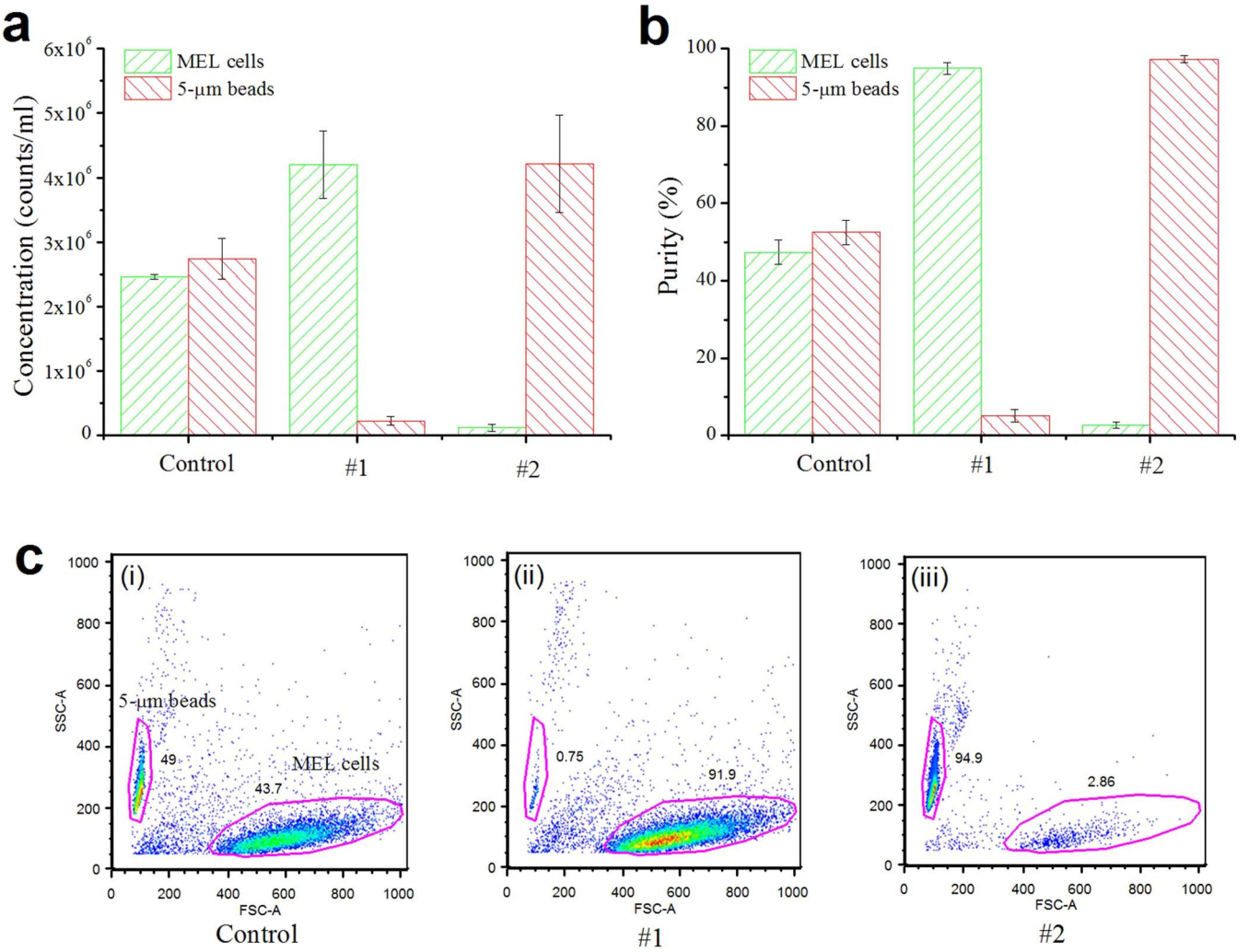

Figure 6 | (a) Concentrations of 5-μm polystyrene beads and MEL cells from control and two outlets under the flow condition of $Re_c = 120$. (b) Purity of 5-μm polystyrene beads and MEL cells before and after a single process by the proposed microfluidic device. (c) Flow cytometric data indicate relative concentration of (i) input mixture of 5-μm polystyrene beads and MEL cells, (ii) collection from outlet #1, and (iii) collection from outlet #2. The number near the gated group represents the percentage of group number on the total particle events.

interaction is negligible. Smaller and larger particles will migrate to their own equilibrium positions without interfering each other. However, in a dense mixture, the interaction and even collision of particles may affect the focusing process and final focusing width.

Examining the transition region II (Fig. 2) more closely, we observed some intriguing phenomena. At the entrance of this region, apart from two-sided focusing streaks, another clear focusing streak arises at the centre of the channel. This central focusing streak is expected to be the initial result of the DC force. From the intensity profile of fluorescent streaks, most particles are located within these three streaks (supplementary Fig. S5). In contrast to the increasing intensity of the central focusing streak, two-sided focusing streaks have decreasing intensity and move closer to the channel centre at an increasing flow rate. The three streaks finally merge together forming a single central focusing streak.

The cut-off size of particles in our device was around 8 μm, equivalent to 20% of the channel height. Demonstrated size difference for particle separation were 7 μm (for 3-μm and 10-μm particles mixture) and 8 μm (for 5-μm and 13-μm particles mixture) respectively. Here we defined that the complete separation happened at the overlap of region I and region III (Fig. 2b). In the actual situation, an efficient separation can still be achieved between region I and region II. In the region II, particles are focused to a band at the channel centre, which have not reached complete focusing. If the lateral distance between this focusing band of large particles and two-sided focusing streaks of small particles is large enough, particle separation can still be achieved with carefully tailored trifurcating outlets. For example, under the condition of a channel Reynolds number of $Re_C = 120$ (Fig. 2a), particles with diameter of 8 μm are focused at the central area of channel with a width of 37 μm. Under the same flow condition, 5-μm particles are focused at the two sides of the channel symmetrically, 58 μm away from channel centre, with each streak width of about 15 μm. So the minimum lateral distance between 8-μm and 5-μm particle streaks is about 32 μm, which is still sufficient for particle separation using the right outlet geometry. Therefore, the actual size difference for complete particle separation could be much smaller, even less than 3 μm.

In our work, due to the assistance from secondary flow, inertial focusing can be achieved within much shorter channel length in a serpentine channel than that in a straight channel[24], therefore leading to a smaller device footprint. Although the throughput of a single serpentine channel demonstrated here is 600 μl/min, which is far less than 1.7 ml/min for a state-of-the art spiral channel[26], it can be easily scaled up by massive parallelization due to its linear structure. For example, a device with eight parallel serpentine channels can reach a throughput of 4.8 ml/min (supplementary Fig. S6). In addition, the

separation performance (purity and efficiency) is improved greatly than the reported asymmetric serpentine channel[3], and even comparable to the most outstanding inertial microfluidic devices[24,29,32]. After a detailed comparison of existing inertial microfluidic techniques to our work (see supplementary Table S1), we can conclude that our device holds an integrative advantage over existing ones, including excellent separation purity and efficiency, good parallelizability, small footprint and high separation resolution, although it is not significantly superior over the existing ones on specific single criteria.

Challenges of our work. Since the inertial lift force, secondary flow drag and particle centrifugal force are all proportional to particle size, inertial focusing and separation performance is quite sensitive to particle size. In our work, we found that focusing performance of small particles (3-μm) is not as good as large particles (10-μm). This can be verified by the fluorescent profile of 3-μm and 10-μm particles at the outlet (Fig. 3c(ii)). The full width at half maximums (FWHM) of 3-μm particles is more than 27 mm, which is 9 times of its particle diameter, while the corresponding FWHM value for 10-μm particles is less than 20 μm, only 2 times of its particle diameter. The wide distribution of 3-μm particles increases the possibility of contamination on large particles collection. That's why the purity of large particle collection is always worse than small particle collection, while the efficiency is often better. In order to acquire high separation performance for both large and small particles, a more efficient way is needed to improve focusing of small particles, e.g. extension of channel length or modification of channel dimension. Additionally, before separation, quite a lot of tests are needed to determine exact thresholds of three focusing patterns for each sized particles, then to determine available flow condition for separation of specific particles mixture. However, this kind of calibration is necessary for all the inertial microfludic devices until the exact mechanism of inertial focusing process is uncovered.

In conclusion, the proposed inertial microfluidic device is expected to be a good alternative for the conventional separation devices. And it promises a cost-effective, label free and robust method for cell preparation and clinical diagnosis.

Methods

Device fabrication. Based on our previous study of particle inertial focusing[47], we implemented a trifurcating outlet at the end of the channel, so that three different particle streaks could be collected in the corresponding branches. The two-sided symmetrical bifurcations were combined to a single outlet to simplify handling. The device with a single serpentine channel has a footprint of 36 mm × 5 mm. The device was fabricated by standard photolithography and soft lithography techniques. The detailed fabricating procedure was given elsewhere[53].

Cell culture. Murine erythroleukemia (MEL) cells were maintained in a complete culture medium (RPMI-1640 medium containing 10% fetal calf serum and 2 mM L-glutamine) at 37°C and 95% air/5% CO_2 as previously described[54]. In order to visualise the trajectory of MEL cells in the microfluidic device, MEL cells were labelled using PKH26 red fluorescent cell linker kit (Sigma-Aldrich, Product No. P9691) according to the manufacturer's instructions as follows. Cell clusters were removed using a 70-μm cell strainer (Becton Dickinson, Product No. 352350) and the single cell suspension was washed twice with serum-free RPMI-1640 medium (400 × g for 5 min at 22°C). Cells (2×10^7) were then resuspended in 1 ml of Diluent C (Product No. G8278) and rapidly mixed with 1 ml of Diluent C containing 2×10^{-6} M PKH26 ethanolic dye solution (Product No. P9691). Immediately following mixing, 2 ml of fetal calf serum was added, and the mixture was incubated for 1 min. The cells were then washed three times in 10 ml of complete medium (400 × g for 5 min at 22°C) and finally suspended in the complete medium at $\sim 4.4 \times 10^6$ cells/ml.

Particle preparation. Fluorescent polystyrene particles were purchased from Thermo Fisher Scientific. Particles with a mean diameter of a = 3.2 μm (Product No. R0300, CV5%), 4.8 μm (Product No. G0500, CV5%), 8 μm (Product No. 36–3, CV18%), 9.9 μm (Product No. G1000, CV5%) and 13 μm (Product No. 36–4, CV16%) were suspended respectively in deionized (DI) water. Tween 20 (Sigma-Aldrich, Product No. P9416) with 0.1% w/v was added to prevent particles from aggregation. The weight ratio of particles in the suspension was 0.05%. To conduct the separation of polystyrene beads mixtures, two pairs of beads mixture (3-μm/10-μm beads mixture, and 5-μm/13-μm beads mixture) were prepared in DI water with 0.1% w/v tween. Their concentrations were listed in Figures 4b and 5b. For testing mixture of MEL cells and 5-μm polystyrene beads in the proposed device, 5-μm polystyrene beads and PKH26-labelled MEL cells were mixed by a ratio of ~ 1 : 1, and suspended in phosphate-buffered saline (PBS) with a MEL cell concentration of $\sim 2.46 \times 10^6$/ml. The whole blood was donated from a healthy male. The MEL cells were spiked into the whole blood sample, with a ratio of ~1 : 100 for the separation of MEL cells from whole blood. The mixture was diluted by PBS to the concentration of the whole cells around 7.5×10^7 counts/ml.

Experimental setup and method. The microfluidic device was placed on an inverted microscope (CKX41, Olympus), illuminated by a mercury arc lamp. Particle suspension was pumped by a syringe pump (Legato 100, KD Scientific). The fluorescent images were observed and captured by a CCD camera (Rolera Bolt, Q-imaging), and then post-processed and analysed using the software Q-Capture Pro 7 (Q-imaging). The exposure time for each frame was kept constant at 100 ms. The concentrations of particles and cells were measured by a hemocytometry. The purity of particle suspensions collected from different outlets was calculated from three measurements by hemocytometry. An LSR II flow cytometer (BD Biosciences) was used to further verify the purity from two collections. The flow cytometer data was analysed using FlowJo software (Tree Star).

1. Jin, C. *et al.* Technologies for label-free separation of circulating tumor cells: from historical foundations to recent developments. *Lab Chip* **14**, 32–44 (2014).
2. Bhagat, A. A. S., Hou, H. W., Li, L. D., Lim, C. T. & Han, J. Pinched flow coupled shear-modulated inertial microfluidics for high-throughput rare blood cell separation. *Lab Chip* **11**, 1870–1878 (2011).
3. Di Carlo, D., Edd, J. F., Irimia, D., Tompkins, R. G. & Toner, M. Equilibrium separation and filtration of particles using differential inertial focusing. *Anal. Chem.* **80**, 2204–2211 (2008).
4. Fukuda, S. & Schmid-Schönbein, G. W. Centrifugation attenuates the fluid shear response of circulating leukocytes. *J. Leukoc. Biol.* **72**, 133–139 (2002).
5. Xie, Y. *et al.* The effect of centrifugation on viability of fat grafts: an evaluation with the glucose transport test. *J. Plast. Reconstr. Aesthet. Surg.* **63**, 482–487 (2010).
6. Gossett, D. R. *et al.* Label-free cell separation and sorting in microfluidic systems. *Anal. Bioanal. Chem.* **397**, 3249–3267 (2010).
7. Pamme, N. Continuous flow separations in microfluidic devices. *Lab Chip* **7**, 1644–1659 (2007).
8. Çetin, B. & Li, D. Dielectrophoresis in microfluidics technology. *Electrophoresis* **32**, 2410–2427 (2011).
9. Li, M., Li, S., Li, W., Wen, W. & Alici, G. Continuous manipulation and separation of particles using combined obstacle-and curvature-induced direct current dielectrophoresis. *Electrophoresis* **34**, 952–960 (2013).
10. Forbes, T. P. & Forry, S. P. Microfluidic magnetophoretic separations of immunomagnetically labeled rare mammalian cells. *Lab Chip* **12**, 1471–1479 (2012).
11. Shen, F., Hwang, H., Hahn, Y. K. & Park, J. K. Label-Free Cell Separation Using a Tunable Magnetophoretic Repulsion Force. *Anal. Chem.* **84**, 3075–3081 (2012).
12. Li, S. *et al.* An on-chip, multichannel droplet sorter using standing surface acoustic waves (SSAW). *Anal. Chem.* **85**, 5468–5474 (2013).
13. Destgeer, G., Lee, K. H., Jung, J. H., Alazzam, A. & Sung, H. J. Continuous separation of particles in a PDMS microfluidic channel via travelling surface acoustic waves (TSAW). *Lab Chip* **13**, 4210–4216 (2013).
14. MacDonald, M., Spalding, G. & Dholakia, K. Microfluidic sorting in an optical lattice. *Nature* **426**, 421–424 (2003).
15. Jung, J. H. *et al.* Optical separation of droplets on a microfluidic platform. *Microfluid. Nanofluid.* 1–10 (2013).
16. Ji, H. M. *et al.* Silicon-based microfilters for whole blood cell separation. *Biomed. Microdevices* **10**, 251–257 (2008).
17. Yamada, M., Nakashima, M. & Seki, M. Pinched flow fractionation: continuous size separation of particles utilizing a laminar flow profile in a pinched microchannel. *Anal. Chem.* **76**, 5465–5471 (2004).
18. Huang, L. R., Cox, E. C., Austin, R. H. & Sturm, J. C. Continuous particle separation through deterministic lateral displacement. *Science* **304**, 987–990 (2004).
19. Choi, S. & Park, J. K. Continuous hydrophoretic separation and sizing of microparticles using slanted obstacles in a microchannel. *Lab Chip* **7**, 890–897 (2007).
20. Di Carlo, D. Inertial microfluidics. *Lab Chip* **9**, 3038–3046 (2009).
21. Segre, G. Radial particle displacements in Poiseuille flow of suspensions. *Nature* **189**, 209–210 (1961).
22. Di Carlo, D., Irimia, D., Tompkins, R. G. & Toner, M. Continuous inertial focusing, ordering, and separation of particles in microchannels. *Proc. Natl. Acad. Sci. U.S.A.* **104**, 18892 (2007).
23. Hur, S. C., Brinckerhoff, T. Z., Walthers, C. M., Dunn, J. C. & Di Carlo, D. Label-free enrichment of adrenal cortical progenitor cells using inertial microfluidics. *PLoS One* **7**, e46550 (2012).
24. Zhou, J., Giridhar, P. V., Kasper, S. & Papautsky, I. Modulation of aspect ratio for complete separation in an inertial microfluidic channel. *Lab Chip* **13**, 1919–1929 (2013).
25. Zhou, J. & Papautsky, I. Fundamentals of inertial focusing in microchannels. *Lab Chip* **13**, 1121–1132 (2013).
26. Warkiani, M. E. *et al.* Slanted spiral microfluidics for the ultra-fast, label-free isolation of circulating tumor cells. *Lab Chip* **14**, 128–137 (2014).

27. Sollier, E. *et al.* Size-selective collection of circulating tumor cells using Vortex technology. *Lab Chip* **14**, 63–77 (2014).
28. Mach, A. J. & Di Carlo, D. Continuous scalable blood filtration device using inertial microfluidics. *Biotechnol. Bioeng.* **107**, 302–311 (2010).
29. Lee, M. G., Shin, J. H., Bae, C. Y., Choi, S. & Park, J.-K. Label-Free Cancer Cell Separation from Human Whole Blood Using Inertial Microfluidics at Low Shear Stress. *Anal. Chem.* **85**, 6213–6218 (2013).
30. Zhang, J., Li, M., Li, W. H. & Alici, G. Inertial focusing in a straight channel with asymmetrical expansion–contraction cavity arrays using two secondary flows. *J. Micromech. Microeng.* **23**, 085023 (2013).
31. Bhagat, A. A. S., Kuntaegowdanahalli, S. S. & Papautsky, I. Continuous particle separation in spiral microchannels using dean flows and differential migration. *Lab Chip* **8**, 1906–1914 (2008).
32. Lee, M. G., Choi, S. & Park, J. K. Inertial separation in a contraction–expansion array microchannel. *J. Chromatogr. A* **1218**, 4138–4143 (2011).
33. Lee, M. G. *et al.* Inertial blood plasma separation in a contraction–expansion array microchannel. *Appl. Phys. Lett.* **98**, 253702–253702–253703 (2011).
34. Mach, A. J., Kim, J. H., Arshi, A., Hur, S. C. & Di Carlo, D. Automated cellular sample preparation using a Centrifuge-on-a-Chip. *Lab Chip* **11**, 2827–2834 (2011).
35. Zhou, J., Kasper, S. & Papautsky, I. Enhanced size-dependent trapping of particles using microvortices. *Microfluid. Nanofluid.* 1–13 (2013).
36. Wang, X., Zhou, J. & Papautsky, I. Vortex-aided inertial microfluidic device for continuous particle separation with high size-selectivity, efficiency, and purity. *Biomicrofluid* **7**, 044119 (2013).
37. Che, J. *et al.* Microfluidic purification and concentration of malignant pleural effusions for improved molecular and cytomorphological diagnostics. *PLoS One* **8**, e78194 (2013).
38. Kuntaegowdanahalli, S. S., Bhagat, A. A. S., Kumar, G. & Papautsky, I. Inertial microfluidics for continuous particle separation in spiral microchannels. *Lab Chip* **9**, 2973–2980 (2009).
39. Yoon, D. H. *et al.* Size-selective separation of micro beads by utilizing secondary flow in a curved rectangular microchannel. *Lab Chip* **9**, 87–90 (2008).
40. Sun, J. *et al.* Double spiral microchannel for label-free tumor cell separation and enrichment. *Lab Chip* **12**, 3952–3960 (2012).
41. Sun, J. *et al.* Size-based hydrodynamic rare tumor cell separation in curved microfluidic channels. *Biomicrofluid* **7**, 011802 (2013).
42. Hou, H. W. *et al.* Isolation and retrieval of circulating tumor cells using centrifugal forces. *Sci. Rep.* **3**, 1259 (2013).
43. Guan, G. *et al.* Spiral microchannel with rectangular and trapezoidal cross-sections for size based particle separation. *Sci. Rep.* **3** (2013).
44. Wu, L., Guan, G., Hou, H. W., Bhagat, A. A. S. & Han, J. Separation of Leukocytes from Blood Using Spiral Channel with Trapezoid Cross-Section. *Anal. Chem.* **84**, 9324–9331 (2012).
45. Gossett, D. R. & Carlo, D. D. Particle focusing mechanisms in curving confined flows. *Anal. Chem.* **81**, 8459–8465 (2009).
46. Ozkumur, E. *et al.* Inertial Focusing for Tumor Antigen–Dependent and–Independent Sorting of Rare Circulating Tumor Cells. *Sci. Transl. Med.* **5**, 179ra147–179ra147 (2013).
47. Zhang, J., Li, W., Li, M., Alici, G. & Nguyen, N.-T. Particle inertial focusing and its mechanism in a serpentine microchannel. *Microfluid. Nanofluid.* 1–12, doi: 10.1007/s10404-013-1306-6 (2013).
48. Chung, A. J., Gossett, D. R. & Di Carlo, D. Three Dimensional, Sheathless, and High-Throughput Microparticle Inertial Focusing Through Geometry-Induced Secondary Flows. *Small* **9**, 685–690 (2013).
49. Loutherback, K. *et al.* Deterministic separation of cancer cells from blood at 10 mL/min. *AIP advances* **2**, 042107 (2012).
50. Wang, B. & Sluyter, R. P2X7 receptor activation induces reactive oxygen species formation in erythroid cells. *Purinergic Signal.* **9**, 101–112 (2013).
51. Friend, C., Scher, W., Holland, J. & Sato, T. Hemoglobin synthesis in murine virus-induced leukemic cells in vitro: stimulation of erythroid differentiation by dimethyl sulfoxide. *Proc. Natl. Acad. Sci. U.S.A.* **68**, 378–382 (1971).
52. Tsiftsoglou, A. S., Pappas, I. S. & Vizirianakis, I. S. Mechanisms involved in the induced differentiation of leukemia cells. *Pharmacol. Ther.* **100**, 257–290 (2003).
53. Duffy, D. C., McDonald, J. C., Schueller, O. J. A. & Whitesides, G. M. Rapid prototyping of microfluidic systems in poly (dimethylsiloxane). *Anal. Chem.* **70**, 4974–4984 (1998).
54. Constantinescu, P. *et al.* P2X7 receptor activation induces cell death and microparticle release in murine erythroleukemia cells. *Biochim. Biophys. Acta* **1798**, 1797–1804 (2010).

Acknowledgments

This work was partially supported by the University of Wollongong through a UIC grant and China Scholarship Council. Special thanks are given to Ms. Aleta Pupovac for the technical assistance with MEL cell cultures and dye staining.

Author contributions

J.Z., W.L., G.A. and N.T.N. designed research. J.Z. and S.Y. conducted experiments and analysed the data. R.S. contributed reagents and the MEL cell sample, and provided technical assistance on flow cytometer test. J.Z., W.L. and N.T.N. co-wrote the manuscript. All the authors have reviewed the manuscript.

Additional information

Supplementary information accompanies this paper at http://www.nature.com/scientificreports

Competing financial interests: The authors declare no competing financial interests.

How to cite this article: Zhang, J. *et al.* Inertial particle separation by differential equilibrium positions in a symmetrical serpentine micro-channel. *Sci. Rep.* **4**, 4527; DOI:10.1038/srep04527 (2014).